Computational Mechanics (1993) 12, 147–163

Computational Mechanics

A hybrid brick element with rotational degrees of freedom

K. Y. Sze[1] and A. Ghali[2]

[1] School of Mechanical and Production Engineering, Nanyang Technological University, Nanyang Avenue, Singapore 2263
[2] Department of Civil Engineering, University of Calgary, 2500 University Drive N.W., Calgary, Alberta, Canada T2N 1N4

Abstract. An 8-node brick element using Allman's displacement interpolation is proposed. The optimal number of 36 stress modes is identified. The six *equal-rotation* strainless modes which are intrinsic to Allman's interpolation are stabilized by using a penalty method. The penalty also enforces the equality of the nodal rotation and the continuum-defined rotation. To enhance computational efficiency, 39 stress modes are initially assumed, three constraints on the stress field are then imposed. The flexibility matrix is simplified, such that only four symmetric 3×3 matrices are required to be inverted. Numerical test results are presented, showing good accuracy.

1 Introduction

Finite element researchers have long been aware of the importance of membrane elements with factual inplane torsional stiffness. These elements are very useful for modeling spatial structures such as tubular joints, girder boxes and folded plates. Unfortunately, early attempts in deriving these elements were not successful. Irons and Ahmad (1980) even pointed out that inclusion of inplane rotations always leads to patch test failure. Nevertheless, a break through was achieved by Allman (1984) and Bergan and Felippa (1985).

Allman adopted a quadratic interpolation scheme for the deformed element boundary in lieu of the conventional cubic beam function. The same scheme was soon applied to various structural elements (Cook 1986; MacNeal and Harder 1989; Pawlak et al. 1991; Ibrahimbegovic and Wilson 1991; Sze et al. 1992). However, the scheme is not defect-free. First, the nodal rotation used in Allman's interpolation is not in conformity with the continuum-defined rotation (Allman 1984). Secondly, some strainless modes, which will be referred to as the *equal-rotation* modes (MacNeal and Harder 1989), can be observed when all the nodal rotations about any particular axis assume the same value. For membrane elements, the mechanism does not plague practical analyses, since it can be suppressed by restraining any one of nodal rotations in a mesh. However, the situation in brick elements becomes much more complicated, and a built-in stabilization scheme should be used.

Recent emphasis on elements with rotational d.o.f. is on the conformity of the nodal rotation with the continuum-defined rotation, especially when nodal couples (the energy conjugate of the nodal rotation) are prescribed. This is of prime importance when solid elements are interfaced with plate, shell or beam elements. The interfacing is traditionally handled in a laborious way by defining constraint equations (Cook et al. 1989).

The intent of the present paper is to develop a robust and accurate 8-node hybrid brick element with Allman's rotational d.o.f. A penalty method which enforces the equality of the nodal rotation and the continuum-defined rotation is used. *Admissible matrix formulation* will be adopted, to simplify the element's flexibility matrix (Sze 1992) for enhanced computational efficiency.

2 Hellinger–Reissner functional with penalty

Precursors of the employed functional can be found in Reissner (1986), Hughes and Brezzi (1989) and Iura and Atluri (1992). As shown in the last reference, Iura and Atluri's functional for elasticity problem was derived from Atluri's earlier works on large strain problems (Atluri 1979, 1980). To derive the present functional, one may condense the skew symmetric stress components from any of the precursors and write:

$$\Pi^e = \int_{v^e} (-\tfrac{1}{2}\underline{\sigma}^{\mathrm{T}}\mathbf{S}\underline{\sigma} + \underline{\sigma}^{\mathrm{T}}\mathbf{L}_t\mathbf{u} - \mathbf{b}^{\mathrm{T}}\mathbf{u})\,dv - \int_{St^e} \bar{\mathbf{t}}^{\mathrm{T}}\mathbf{u}\,ds + \tfrac{1}{2}\gamma \int_{v^e} (\underline{\Omega} - \underline{\omega})^2\,dv \tag{1}$$

where $\underline{\sigma} = [\sigma_x\ \sigma_y\ \sigma_z\ \sigma_{xy}\ \sigma_{yz}\ \sigma_{zx}]^{\mathrm{T}}$ is the vectorial representation of the assumed symmetric stress tensor, $\mathbf{S}$ is material compliance matrix; $\mathbf{L}_t$ is strain-displacement differential operator; $\mathbf{u} = [u\ v\ w]^{\mathrm{T}}$ is the translational displacement vector; $\mathbf{b}$ is the body force vector; v^e is the element domain; St^e is the portion of the element boundary over which the surface traction $\bar{\mathbf{t}}$ is prescribed; $\underline{\omega} = [\omega_x\ \omega_y\ \omega_z]^{\mathrm{T}}$ is the vector containing the independent assumed rotations; $\underline{\Omega} = [\Omega_x\ \Omega_y\ \Omega_z]^{\mathrm{T}}$ is the continuum-defined rotation, namely

$$\underline{\Omega}^u = \begin{Bmatrix} \Omega_x \\ \Omega_y \\ \Omega_z \end{Bmatrix} = \frac{1}{2} \begin{bmatrix} 0 & -\dfrac{\partial}{\partial z} & \dfrac{\partial}{\partial y} \\ \dfrac{\partial}{\partial z} & 0 & -\dfrac{\partial}{\partial x} \\ -\dfrac{\partial}{\partial y} & \dfrac{\partial}{\partial x} & 0 \end{bmatrix} \begin{Bmatrix} u \\ v \\ w \end{Bmatrix} = \mathbf{L}_r\mathbf{u}. \tag{2}$$

Lastly, γ is the penalty scalar for enforcing the equality of $\underline{\omega}$ and $\underline{\Omega}$. The functional is no different from the conventional Hellinger–Reissner functional except for the last penalty integral.

3 Interpolation for displacements and rotations

Figure 1 shows an 8-node hexahedral element. According to Allman's (1984) scheme, the x-translational displacement of the fictitious mid-side point bounded by its two adjacent corner nodes i and j is:

$$u = \frac{1}{2}(u_i + u_j) + \frac{y_j - y_i}{8}(\omega_{zj} - \omega_{zi}) - \frac{z_j - z_i}{8}(\omega_{yj} - \omega_{yi}) \tag{3}$$

in which quantities with suffixes refer to their nodal values. Other translational displacement components can be obtained by cyclic symmetry (Yunus et al. 1989). With the translations of the midside points thus determined, the displacement field is interpolated by using the interpolation

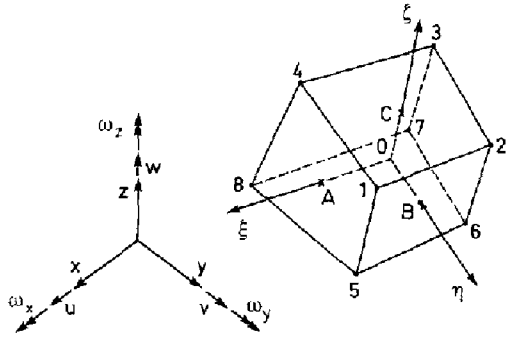

Fig. 1. Eight-node hexahedral element

functions of the standard 20-node brick element. After some simple algebra, we have:

$$\mathbf{u} = \begin{Bmatrix} u \\ v \\ w \end{Bmatrix} = \mathbf{N}_t \begin{Bmatrix} \mathbf{q}_1 \\ \vdots \\ \mathbf{q}_8 \end{Bmatrix} \mathbf{q} = \mathbf{N}_t \mathbf{q} \tag{4}$$

in which $\mathbf{q}_i = [u_i \; v_i \; w_i \; \omega_{xi} \; \omega_{yi} \; \omega_{zi}]^T$ and the interpolation matrix $\mathbf{N}_t$ is given explicitly in the Appendix. Strain can then be derived:

$$\underline{\varepsilon} = \begin{Bmatrix} \varepsilon_{xx} \\ \varepsilon_{yy} \\ \varepsilon_{zz} \\ 2\varepsilon_{xy} \\ 2\varepsilon_{yz} \\ 2\varepsilon_{zx} \end{Bmatrix} = \begin{bmatrix} \frac{\partial}{\partial x} & 0 & 0 \\ 0 & \frac{\partial}{\partial y} & 0 \\ 0 & 0 & \frac{\partial}{\partial z} \\ \frac{\partial}{\partial y} & \frac{\partial}{\partial x} & 0 \\ 0 & \frac{\partial}{\partial z} & \frac{\partial}{\partial y} \\ \frac{\partial}{\partial z} & 0 & \frac{\partial}{\partial x} \end{bmatrix} \begin{Bmatrix} u \\ v \\ w \end{Bmatrix} = \mathbf{L}_t \mathbf{u} = \mathbf{L}_t \mathbf{N}_t \mathbf{q}. \tag{5}$$

The continuum-defined rotation is obtained by combining Eq. (2) and Eq. (4),

$$\underline{\Omega} = \mathbf{L}_r \mathbf{u} = \mathbf{L}_r \mathbf{N}_t \mathbf{q}. \tag{6}$$

The independently assumed rotation is interpolated using the nodal rotations and the standard trilinear shape functions of the 8-node element, i.e.

$$\underline{\omega} = [\mathbf{0}_{3\times 3} \; N_1\mathbf{I}_3 \; \mathbf{0}_{3\times 3} \; N_2\mathbf{I}_3 \; \cdots \; \mathbf{0}_{3\times 3} \; N_7\mathbf{I}_3 \; \mathbf{0}_{3\times 3} \; N_8\mathbf{I}_3]\mathbf{q} = \mathbf{N}_r \mathbf{q}. \tag{7}$$

Interpolation functions N_1 to N_8 can be found in the Appendix.

4 Geometric parameters

Referring to Fig. 1, the following geometric parameters are defined for the sake of convenience:

$$\begin{bmatrix} a_1 & b_1 & c_1 \\ a_2 & b_2 & c_2 \\ a_3 & b_3 & c_3 \end{bmatrix} = \frac{1}{8} \begin{bmatrix} 1 & -1 & -1 & 1 & 1 & -1 & -1 & 1 \\ 1 & 1 & -1 & -1 & 1 & 1 & -1 & -1 \\ 1 & 1 & 1 & 1 & -1 & -1 & -1 & -1 \end{bmatrix} \begin{bmatrix} x_1 & y_1 & z_1 \\ \vdots & \vdots & \vdots \\ x_8 & y_8 & z_8 \end{bmatrix} \tag{8a}$$

$$\begin{bmatrix} A_1 & A_2 & A_3 \\ B_1 & B_2 & B_3 \\ C_1 & C_2 & C_3 \end{bmatrix} = \begin{bmatrix} a_1 & b_1 & c_1 \\ a_2 & b_2 & c_2 \\ a_3 & b_3 & c_3 \end{bmatrix}^{-1} \tag{8b}$$

and

$$\{f_0 \; f_1 \; f_2 \; f_3 \; f_4 \; f_5 \; f_6 \; f_7 \; f_8 \; f_9 \; f_{10} \; f_{11} \; f_{12} \; f_{13} \; f_{14} \; f_{15}\} = \int_{v^e} \{1 \; \xi \; \eta \; \zeta \; \eta\zeta \; \zeta\xi \; \xi\eta \; \xi^2 \; \eta^2 \; \zeta^2 \; \zeta\xi^2 \; \xi\eta^2 \; \eta\zeta^2 \; \eta\xi^2 \; \zeta\eta^2 \; \xi\zeta^2\} dv. \tag{9}$$

All f_i's can be evaluated by symbolic computation with minor effort.

5 Stress shape functions

Without ambiguity, stress from now on would refer only to the symmetric one. Since it is easier to maintain element invariance by using contravariant stress modes (Rubinstein et al. 1983; Pian and Sumihara 1984; Punch and Atluri 1984; Sze et al. 1992), they will be adopted in the present element. An important role of a chosen stress field is to stabilize the associated element. To avoid an overstiff element and reduce computing time, the number of stress modes should preferably be kept minimum which is taken as the difference between the number of nodal d.o.f. and the number of rigid body modes (Pian and Tong 1969; Pian and Chen 1983; Rubinstein et al. 1983). The physical idea behind this is to match each of the deformation modes, in which strain is non-zero, by one stress mode. For the present element, there are 48 nodal d.o.f. and since the 6 rigid body modes and the 6 *equal-rotation* modes (Yunus et al. 1991) are strainless modes, the minimum number of stress modes would be 36.

To observe what stress modes can stabilize the element and at the same time are compatible to the deformation modes, the displacement-derived strain of a quadrilateral with drilling d.o.f. is examined. This element has 12 nodal d.o.f., 3 rigid body modes and 1 *equal-rotation* mode, the minimum number of stress modes is 8. Consider a bi-unit square element with its x-and y-axes parallel to the ξ- and η-axes respectively, its displacement field can be expressed as (Sze et al. 1992):

$$u = U_0 + U_1\xi + U_2\eta + U_3\xi\eta + U_4\eta^2 + U_5\xi\eta^2, \quad v = V_0 + V_1\xi + V_2\eta + V_3\xi\eta + V_4\xi^2 + V_5\xi^2\eta \qquad (10a, b)$$

in which U_i's and V_i's are linear functions of the nodal d.o.f., and $U_5 + V_5 = 0$. The derived strain is:

$$\varepsilon_{\xi\xi} = \frac{\partial u}{\partial \xi} = U_1 + U_3\eta + U_5\eta^2; \quad \varepsilon_{\eta\eta} = \frac{\partial v}{\partial \eta} = V_2 + V_3\xi - U_5\xi^2 \qquad (11a)$$

$$2\varepsilon_{\xi\eta} = \frac{\partial u}{\partial \eta} + \frac{\partial v}{\partial \xi} = U_2 + V_1 + (U_3 + 2V_4)\xi + (2U_4 + V_3)\eta. \qquad (11b)$$

All the deformation modes can be stabilized by 3 constant stress modes plus the following 5 higher order contravariant stress modes (Sze and Ghali 1992):

$$\begin{Bmatrix} \sigma^{\xi\xi} \\ \sigma^{\eta\eta} \\ \sigma^{\xi\eta} \end{Bmatrix}_h = \begin{bmatrix} \eta & 0 & 0 & 0 & \eta^2 \\ 0 & \xi & 0 & 0 & -\xi^2 \\ 0 & 0 & \eta & \xi & 0 \end{bmatrix} \underline{\beta}_h \qquad (12)$$

where $\underline{\beta}_h$ represents a vector of coefficients for higher order stress modes. The higher order stress modes for the brick element can now be derived by using Eq. (12) as the hierarchic building block. As there are two layers of nodes in the ζ-direction, a linear variation of $[\sigma^{\xi\xi} \ \sigma^{\eta\eta} \ \sigma^{\xi\eta}]_h^T$ should be assumed, i.e.

$$\begin{Bmatrix} \sigma^{\xi\xi} \\ \sigma^{\eta\eta} \\ \sigma^{\xi\eta} \end{Bmatrix}_h = \left(\begin{bmatrix} \eta & 0 & 0 & 0 & \eta^2 \\ 0 & \xi & 0 & 0 & -\xi^2 \\ 0 & 0 & \xi & \eta & 0 \end{bmatrix} + \zeta \begin{bmatrix} \eta & 0 & 0 & 0 & \eta^2 \\ 0 & \xi & 0 & 0 & -\xi^2 \\ 0 & 0 & \xi & \eta & 0 \end{bmatrix} \right) \underline{\beta}_h. \qquad (13a)$$

Seemingly, for the layers of nodes in the ξ- and η-directions, we have:

$$\begin{Bmatrix} \sigma^{\eta\eta} \\ \sigma^{\zeta\zeta} \\ \sigma^{\eta\zeta} \end{Bmatrix}_h = \left(\begin{bmatrix} \zeta & 0 & 0 & 0 & \zeta^2 \\ 0 & \eta & 0 & 0 & -\eta^2 \\ 0 & 0 & \eta & \zeta & 0 \end{bmatrix} + \xi \begin{bmatrix} \zeta & 0 & 0 & 0 & \zeta^2 \\ 0 & \eta & 0 & 0 & -\eta^2 \\ 0 & 0 & \eta & \zeta & 0 \end{bmatrix} \right) \underline{\beta}_h \qquad (13b)$$

and

$$\begin{Bmatrix} \sigma^{\zeta\zeta} \\ \sigma^{\xi\xi} \\ \sigma^{\zeta\xi} \end{Bmatrix}_h = \left(\begin{bmatrix} \xi & 0 & 0 & 0 & \xi^2 \\ 0 & \zeta & 0 & 0 & -\zeta^2 \\ 0 & 0 & \zeta & \xi & 0 \end{bmatrix} + \eta \begin{bmatrix} \xi & 0 & 0 & 0 & \xi^2 \\ 0 & \zeta & 0 & 0 & -\zeta^2 \\ 0 & 0 & \zeta & \xi & 0 \end{bmatrix} \right) \underline{\beta}_h. \qquad (13c)$$

By combining the last three equations with the redundant modes deleted, the 30 higher order contravariant stress modes are:

$$\underline{\sigma}_{\text{contravariant}} = \begin{Bmatrix} \sigma^{\xi\xi} \\ \sigma^{\eta\eta} \\ \sigma^{\zeta\zeta} \\ \sigma^{\xi\eta} \\ \sigma^{\eta\zeta} \\ \sigma^{\zeta\xi} \end{Bmatrix}_h = [\xi\bar{\mathbf{P}}_1 \quad \eta\bar{\mathbf{P}}_2 \quad \zeta\bar{\mathbf{P}}_3 \quad \bar{\mathbf{P}}_4 \quad \bar{\mathbf{P}}_5 \quad \bar{\mathbf{P}}_6 \quad \bar{\mathbf{P}}_7 \quad \bar{\mathbf{P}}_8 \quad \bar{\mathbf{P}}_9 \quad \bar{\mathbf{P}}_{10}]\underline{\beta}_h \tag{14}$$

where

$$\bar{\mathbf{P}}_1 = \begin{bmatrix} 0 & 0 & 0 & 0 & 0 \\ 1 & 0 & 0 & 0 & 0 \\ 0 & 1 & 0 & 0 & 0 \\ 0 & 0 & 1 & 0 & 0 \\ 0 & 0 & 0 & 1 & 0 \\ 0 & 0 & 0 & 0 & 1 \end{bmatrix}; \quad \bar{\mathbf{P}}_2 = \begin{bmatrix} 1 & 0 & 0 & 0 & 0 \\ 0 & 0 & 0 & 0 & 0 \\ 0 & 1 & 0 & 0 & 0 \\ 0 & 0 & 1 & 0 & 0 \\ 0 & 0 & 0 & 1 & 0 \\ 0 & 0 & 0 & 0 & 1 \end{bmatrix}; \quad \bar{\mathbf{P}}_3 = \begin{bmatrix} 1 & 0 & 0 & 0 & 0 \\ 0 & 1 & 0 & 0 & 0 \\ 0 & 0 & 0 & 0 & 0 \\ 0 & 0 & 1 & 0 & 0 \\ 0 & 0 & 0 & 1 & 0 \\ 0 & 0 & 0 & 0 & 1 \end{bmatrix}$$

$$\bar{\mathbf{P}}_4 = \begin{bmatrix} 0 & 0 & 0 \\ \zeta\xi & 0 & 0 \\ 0 & 0 & 0 \\ 0 & \zeta\xi & 0 \\ 0 & 0 & \zeta\xi \\ 0 & 0 & 0 \end{bmatrix}; \quad \bar{\mathbf{P}}_5 = \begin{bmatrix} \eta\zeta & 0 & 0 \\ 0 & 0 & 0 \\ 0 & 0 & 0 \\ 0 & \eta\zeta & 0 \\ 0 & 0 & 0 \\ 0 & 0 & \eta\zeta \end{bmatrix}; \quad \bar{\mathbf{P}}_6 = \begin{bmatrix} 0 & 0 & 0 \\ 0 & 0 & 0 \\ \xi\eta & 0 & 0 \\ 0 & 0 & 0 \\ 0 & \xi\eta & 0 \\ 0 & 0 & \xi\eta \end{bmatrix}$$

$$\bar{\mathbf{P}}_7 = \begin{bmatrix} \eta\eta & 0 & -\zeta\zeta \\ -\xi\xi & \zeta\zeta & 0 \\ 0 & -\eta\eta & \xi\xi \\ 0 & 0 & 0 \\ 0 & 0 & 0 \\ 0 & 0 & 0 \end{bmatrix}; \quad \bar{\mathbf{P}}_8 = \begin{bmatrix} \zeta\eta\eta \\ -\zeta\xi\xi \\ 0 \\ 0 \\ 0 \\ 0 \end{bmatrix}; \quad \bar{\mathbf{P}}_9 = \begin{bmatrix} 0 \\ \xi\zeta\zeta \\ -\xi\eta\eta \\ 0 \\ 0 \\ 0 \end{bmatrix}; \quad \bar{\mathbf{P}}_{10} = \begin{bmatrix} -\eta\zeta\zeta \\ 0 \\ \eta\xi\xi \\ 0 \\ 0 \\ 0 \end{bmatrix}.$$

It is interesting to note the difference between the present 30-β higher order stress field and the 36-β higher order stress field in element *AH* of Yunus et al. (1989). Though six more stress modes are assumed in *AH*, the deformation modes stabilized by $\bar{\mathbf{P}}_8$, $\bar{\mathbf{P}}_9$ and $\bar{\mathbf{P}}_{10}$ cannot be suppressed.

It is possible to make the assumed stress field in Eq. (14) more equilibrating. For instance, the stress mode $[0\ 0\ 0\ \xi\ 0\ 0]^T$ would be more equilibrating should it be changed to $[0\ -\eta\ 0\ \xi\ 0\ 0]^T$. Since not much improvement is yielded by using a more equilibrating field, the derived stress field would be adopted due to its simplicity.

Following the practice of Pian and Sumihara (1984), the higher order cartesian stress is obtained by the transformation matrix evaluated at the element origin. The complete cartesian stress would be:

$$\begin{aligned} \underline{\sigma} &= [\sigma_x \quad \sigma_y \quad \sigma_z \quad \sigma_{xy} \quad \sigma_{yz} \quad \sigma_{zx}]^T = \underline{\beta}_c + \mathbf{T}_\sigma \underline{\sigma}_{\text{contravariant}} \\ &= \underline{\beta}_c + \mathbf{T}_\sigma[\xi\bar{\mathbf{P}}_1 \quad \eta\bar{\mathbf{P}}_2 \quad \zeta\bar{\mathbf{P}}_3 \quad \bar{\mathbf{P}}_4 \quad \bar{\mathbf{P}}_5 \quad \bar{\mathbf{P}}_6 \quad \bar{\mathbf{P}}_7 \quad \bar{\mathbf{P}}_8 \quad \bar{\mathbf{P}}_9 \quad \bar{\mathbf{P}}_{10}]\underline{\beta}_h \end{aligned} \tag{15}$$

in which 6 constant stress modes are introduced by $\underline{\beta}_c$ and thus $\dim(\underline{\beta}_c) = 6$. The transformation matrix $\mathbf{T}_\sigma$ can be derived explicitly as:

$$\mathbf{T}_\sigma = [\mathbf{T}_1 \quad \mathbf{T}_2 \quad \mathbf{T}_3 \quad \mathbf{T}_4 \quad \mathbf{T}_5 \quad \mathbf{T}_6] \tag{16}$$

in which

$$\mathbf{T}_1 = [a_1^2 \quad b_1^2 \quad c_1^2 \quad a_1b_1 \quad b_1c_1 \quad c_1a_1]^T; \quad \mathbf{T}_2 = [a_2^2 \quad b_2^2 \quad c_2^2 \quad a_2b_2 \quad b_2c_2 \quad c_2a_2]^T$$
$$\mathbf{T}_3 = [a_3^2 \quad b_3^2 \quad c_3^2 \quad a_3b_3 \quad b_3c_3 \quad c_3a_3]^T;$$
$$\mathbf{T}_4 = [2a_1a_2 \quad 2b_1b_2 \quad 2c_1c_2 \quad a_1b_2 + a_2b_1 \quad b_1c_2 + b_2c_1 \quad c_1a_2 + c_2a_1]^T$$
$$\mathbf{T}_5 = [2a_2a_3 \quad 2b_2b_3 \quad 2c_2c_3 \quad a_2b_3 + a_3b_2 \quad b_2c_3 + b_3c_2 \quad c_2a_3 + c_3a_2]^T$$
$$\mathbf{T}_6 = [2a_3a_1 \quad 2b_3b_1 \quad 2c_3c_1 \quad a_3b_1 + a_1b_3 \quad b_3c_1 + b_1c_3 \quad c_3a_1 + c_1a_3]^T.$$

The stress modes in Eq. (15) are orthogonalized with respect to the constant modes by carrying out the following replacements:

$$\xi, \eta, \zeta \text{ by } \phi_1 = \xi - \frac{f_1}{f_0}, \quad \phi_2 = \eta - \frac{f_2}{f_0}, \quad \phi_3 = \zeta - \frac{f_3}{f_0};$$

$$\eta\zeta, \zeta\xi, \xi\eta \text{ by } \phi_4 = \eta\zeta - \frac{f_4}{f_0}, \quad \phi_5 = \zeta\xi - \frac{f_5}{f_0}, \quad \phi_6 = \xi\eta - \frac{f_6}{f_0};$$

$$\xi^2, \eta^2, \zeta^2 \text{ by } \phi_7 = \xi^2 - \frac{f_7}{f_0}, \quad \phi_8 = \eta^2 - \frac{f_8}{f_0}, \quad \phi_9 = \zeta^2 - \frac{f_9}{f_0};$$

$$\zeta\xi^2 \text{ to } \phi_{10} = \zeta\xi^2 - \frac{\phi_3}{3} - \frac{f_{10}}{f_0}; \quad \xi\eta^2 \text{ by } \phi_{11} = \xi\eta^2 - \frac{\phi_1}{3} - \frac{f_{11}}{f_0};$$

$$\eta\zeta^2 \text{ to } \phi_{12} = \eta\zeta^2 - \frac{\phi_2}{3} - \frac{f_{12}}{f_0}; \quad \eta\xi^2 \text{ by } \phi_{13} = \eta\xi^2 - \frac{\phi_2}{3} - \frac{f_{13}}{f_0};$$

$$\zeta\eta^2 \text{ to } \phi_{14} = \zeta\eta^2 - \frac{\phi_3}{3} - \frac{f_{14}}{f_0}; \quad \xi\zeta^2 \text{ by } \phi_{15} = \xi\zeta^2 - \frac{\phi_1}{3} - \frac{f_{15}}{f_0}. \tag{17}$$

With the suggested replacements, Eq. (15) can further be expanded as:

$$\underline{\sigma} = \underline{\beta}_c + [\phi_1\mathbf{T}_\sigma\bar{\mathbf{P}}_1 \quad \phi_2\mathbf{T}_\sigma\bar{\mathbf{P}}_2 \quad \phi_3\mathbf{T}_\sigma\bar{\mathbf{P}}_3 \quad \mathbf{P}_4 \quad \mathbf{P}_5 \quad \mathbf{P}_6 \quad \mathbf{P}_7 \quad \mathbf{P}_8 \quad \mathbf{P}_9 \quad \mathbf{P}_{10}]\underline{\beta}_h \tag{18}$$

where

$$\mathbf{P}_4 = \phi_4[\mathbf{T}_2 \quad \mathbf{T}_4 \quad \mathbf{T}_5]; \quad \mathbf{P}_5 = \phi_5[\mathbf{T}_1 \quad \mathbf{T}_4 \quad \mathbf{T}_6]; \quad \mathbf{P}_6 = \phi_6[\mathbf{T}_3 \quad \mathbf{T}_5 \quad \mathbf{T}_6];$$
$$\mathbf{P}_7 = [\phi_8\mathbf{T}_1 - \phi_7\mathbf{T}_2 \quad \phi_9\mathbf{T}_2 - \phi_8\mathbf{T}_3 \quad \phi_7\mathbf{T}_3 - \phi_9\mathbf{T}_1]; \quad \mathbf{P}_8 = [\phi_{14}\mathbf{T}_1 - \phi_{10}\mathbf{T}_2];$$
$$\mathbf{P}_9 = [\phi_{15}\mathbf{T}_2 - \phi_{11}\mathbf{T}_3]; \quad \mathbf{P}_{10} = [\phi_{13}\mathbf{T}_3 - \phi_{12}\mathbf{T}_1].$$

6 Equivalent stress field with constraints

With the stress field given in the Eq. (18), inversion of a 30 × 30 flexibility sub-matrix is required. To reduce this cost, stress constraints would be employed. Though incompatible displacement modes are often used to constrain the initially assumed stress field (Pian et al. 1983; Sze and Chow 1991a), the constraints would be directly incorporated instead of using any incompatible modes (Sze and Chow 1991b) in the present implementation. The unconstrained stress field is taken to be:

$$\sigma = \underline{\beta}_c + \phi_1\mathbf{T}_\sigma\underline{\beta}_1 + \phi_2\mathbf{T}_\sigma\underline{\beta}_2 + \phi_3\mathbf{T}_\sigma\underline{\beta}_3 + \mathbf{P}_4\underline{\beta}_4 + \mathbf{P}_5\underline{\beta}_5 + \mathbf{P}_6\underline{\beta}_6 + \mathbf{P}_7\underline{\beta}_7 + \mathbf{P}_8\beta_8 + \mathbf{P}_9\beta_9 + \mathbf{P}_{10}\beta_{10}$$
$$= \mathbf{I}_c\underline{\beta}_c + \mathbf{P}_h\underline{\beta}_h \tag{19}$$

where $\underline{\beta}_h^T = [\underline{\beta}_1^T \quad \underline{\beta}_2^T \quad \underline{\beta}_3^T \quad \underline{\beta}_4^T \quad \underline{\beta}_5^T \quad \underline{\beta}_6^T \quad \underline{\beta}_7^T \quad \beta_8 \quad \beta_9 \quad \beta_{10}]$. Obviously, this is the same as the stress field in Eq. (18) if the following three constraints are imposed:

$$\mathbf{R}_1^T\underline{\beta}_1 = 0; \quad \mathbf{R}_2^T\underline{\beta}_2 = 0; \quad \mathbf{R}_3^T\underline{\beta}_3 = 0 \tag{20}$$

where $\mathbf{R}_1 = [1\ \mathbf{0}_{1\times 5}]^T$, $\mathbf{R}_2 = [0\ 1\ \mathbf{0}_{1\times 4}]^T$ and $\mathbf{R}_3 = [\mathbf{0}_{1\times 2}\ 1\ \mathbf{0}_{1\times 3}]^T$. As the higher order stress modes have been orthogonalized with respect to the constant modes, substituting Eqs. (5)–(7), (19) and (20) into Eq. (1) yields:

$$\Pi^e = -\frac{f_0}{2}\underline{\beta}_c^T\mathbf{S}\underline{\beta}_c + \underline{\beta}_c^T\mathbf{G}_c\mathbf{q} - \frac{1}{2}\underline{\beta}_h^T\mathbf{H}_h\underline{\beta}_h + \underline{\beta}_h^T\mathbf{G}_h\mathbf{q}$$

$$+ \underline{\beta}_1^T\mathbf{R}_1\lambda_1 + \underline{\beta}_2^T\mathbf{R}_2\lambda_2 + \underline{\beta}_3^T\mathbf{R}_3\lambda_3 - \mathbf{F}^T\mathbf{q} + \frac{1}{2}\mathbf{q}^T\mathbf{K}_s\mathbf{q} \tag{21}$$

in which

$$\mathbf{H}_h = \int_{v^e}\mathbf{P}_h^T\mathbf{S}\mathbf{P}_h dv; \quad \mathbf{G}_h^T = [\mathbf{G}_1^T\ \ \mathbf{G}_2^T\ \ \mathbf{G}_3^T\ \ \mathbf{G}_4^T\ \ \mathbf{G}_5^T\ \ \mathbf{G}_6^T\ \ \mathbf{G}_7^T\ \ \mathbf{G}_8^T\ \ \mathbf{G}_9^T\ \ \mathbf{G}_{10}^T]$$

$$\mathbf{G}_c = \int_{v^e}\mathbf{L}_t\mathbf{N}_t dv; \quad \mathbf{G}_1 = \mathbf{T}_\sigma^T\int_{v^e}\phi_1(\mathbf{L}_t\mathbf{N}_t)dv; \quad \mathbf{G}_2 = \mathbf{T}_\sigma^T\int_{v^e}\phi_2(\mathbf{L}_t\mathbf{N}_t)dv$$

$$\mathbf{G}_3 = \mathbf{T}_\sigma^T\int_{v^e}\phi_3(\mathbf{L}_t\mathbf{N}_t)dv; \quad \mathbf{G}_i = \int_{v^e}\mathbf{P}_i^T(\mathbf{L}_t\mathbf{N}_t)dv \quad \text{for } i = 4 \text{ to } 10$$

$$\mathbf{F} = \int_{v^e}\mathbf{N}_t^T\mathbf{b}dv + \int_{St^e}\mathbf{N}_t^T\bar{\mathbf{t}}ds \quad \text{(the element nodal force vector)}$$

$$\mathbf{K}_s = \gamma\int_{v^e}(\mathbf{L}_r\mathbf{N}_t - \mathbf{N}_r)^T(\mathbf{L}_r\mathbf{N}_t - \mathbf{N}_r)dv \quad \text{(the penalty stiffness)}$$

$\underline{\beta}_i^T\mathbf{R}_i\lambda_i$'s in Π^e represent the stress constraints and λ_i's are the pertinent Lagrange multipliers. Nodal forces and couples for prescribed stress and body force should be computed according to the interpolation matrix $\mathbf{N}_t$ as defined in $\mathbf{F}$ for consistency. It is sufficient to evaluate matrices $\mathbf{H}$'s and $\mathbf{G}$'s by the 14-point integration rule (Irons 1971). The advantage of inducing the constraints on $\underline{\beta}_1$, $\underline{\beta}_2$ and $\underline{\beta}_3$ is now elaborated.

7 Simplification by admissible matrix formulation

Recently, Sze (1992) has proved that entries in the flexibility matrix not coupled with the constant stress modes can be subjected to arbitrary changes provided that the matrix is still positive definite. The resulting element can still pass the generalized patch test (Taylor et al. 1986). The proof offers a clue for *admissible changes* in the flexibility matrix.

To enhance computational efficiency of the present element, all entries that vanish for regular element geometry in the flexibility matrix $\mathbf{H}_h$ are set to zero. As a result of the enforced sparsity, inversion of the matrix can be done in a blockwise manner and the best finite element accuracy which is often observed in regular-shaped elements can be preserved. The suggested *admissible* $\mathbf{H}_h$ would thus be:

$$\mathbf{H}_h = \text{diag}\{\mathbf{H}_1\ \ \mathbf{H}_2\ \ \mathbf{H}_3\ \ \mathbf{H}_4\ \ \mathbf{H}_5\ \ \mathbf{H}_6\ \ \mathbf{H}_7\ \ H_8\ \ H_9\ \ H_{10}\} \tag{22}$$

where

$$\{\mathbf{H}_1\ \ \mathbf{H}_2\ \ \mathbf{H}_3\} = \mathbf{T}_\sigma^T\mathbf{S}\mathbf{T}_\sigma\int_{v^e}\{\phi_1^2\ \ \phi_2^2\ \ \phi_3^2\}dv \quad \text{(order } 6\times 6\text{)}$$

$$\mathbf{H}_i = \int_{v^e}\mathbf{P}_i^T\mathbf{S}\mathbf{P}_i dv \quad \text{for } i = 4 \text{ to } 7 \qquad \text{(order } 3\times 3\text{)}$$

$$\mathbf{H}_i = \int_{v^e}\mathbf{P}_i^T\mathbf{S}\mathbf{P}_i dv \quad \text{for } i = 8 \text{ to } 10 \qquad \text{(scalars).}$$

It can be noted that

$$\{\mathbf{H}_1^{-1}\ \ \mathbf{H}_2^{-1}\ \ \mathbf{H}_3^{-1}\} = \left\{\frac{1}{\int_{v^e}\phi_1^2 dv}\ \frac{1}{\int_{v^e}\phi_2^2 dv}\ \frac{1}{\int_{v^e}\phi_3^2 dv}\right\}\mathbf{T}_\sigma^{-1}\mathbf{S}^{-1}\mathbf{T}_\sigma^{-T} \tag{23}$$

in which

$$\mathbf{T}_\sigma^{-1}=\begin{bmatrix} A_1^2 & A_2^2 & A_3^2 & A_1A_2 & A_2A_3 & A_3A_1 \\ B_1^2 & B_2^2 & B_3^2 & B_1B_2 & B_2B_3 & B_3B_1 \\ C_1^2 & C_2^2 & C_3^2 & C_1C_2 & C_2C_3 & C_3C_1 \\ 2A_1B_1 & 2A_2B_2 & 2A_3B_3 & A_1B_2+B_1A_2 & A_2B_3+B_2A_3 & A_3B_1+B_3A_1 \\ 2B_1C_1 & 2B_2C_2 & 2B_3C_3 & B_1C_2+C_1B_2 & B_2C_3+C_2B_3 & B_3C_1+C_3B_1 \\ 2C_1A_1 & 2C_2A_2 & 2C_3A_3 & C_1A_2+A_1C_2 & C_2A_3+A_2C_3 & C_3A_1+A_3C_1 \end{bmatrix}$$

A_i's, B_i's and C_i's have been defined in Eq. (8b). Computing $\mathbf{H}_1^{-1}, \mathbf{H}_2^{-1}$ and $\mathbf{H}_3^{-1}$ incurs no inversion cost. With the chosen *admissible* $\mathbf{H}_h$, Eq. (21) can be expanded as:

$$\Pi^e = -\frac{f_0}{2}\underline{\beta}_c\mathbf{S}\underline{\beta}_c + \beta_c^{\mathrm{T}}\mathbf{G}_c\mathbf{q} + \sum_{i=1}^{3}\left(-\tfrac{1}{2}\underline{\beta}_i^{\mathrm{T}}\mathbf{H}_i\underline{\beta}_i + \underline{\beta}_i^{\mathrm{T}}\mathbf{G}_i\mathbf{q} + \underline{\beta}_i^{\mathrm{T}}\mathbf{R}_i\lambda_i\right)$$
$$+ \sum_{i=4}^{7}\left(-\tfrac{1}{2}\underline{\beta}_i^{\mathrm{T}}\mathbf{H}_i\underline{\beta}_i + \underline{\beta}_i^{\mathrm{T}}\mathbf{G}_i\mathbf{q}\right) + \sum_{i=8}^{10}\left(-\tfrac{1}{2}\beta_i^{\mathrm{T}}\mathbf{H}_i\beta_i + \beta_i^{\mathrm{T}}\mathbf{G}_i\mathbf{q}\right) - \mathbf{F}^{\mathrm{T}}\mathbf{q} + \tfrac{1}{2}\mathbf{q}^{\mathrm{T}}\mathbf{K}_s\mathbf{q}. \tag{24}$$

Variation of the functional gives:

$$\underline{\beta}_c = \frac{1}{f_0}\mathbf{S}^{-1}\mathbf{G}_c\mathbf{q} \tag{25a}$$

$$\underline{\beta}_i = \mathbf{H}_i^{-1}(\mathbf{G}_i\mathbf{q} + \mathbf{R}_i\lambda_i);\quad \mathbf{R}_i^{\mathrm{T}}\beta_i = 0 \quad \text{for } i = 1, 2 \text{ and } 3 \tag{25b}$$

$$\underline{\beta}_i = \mathbf{H}_i^{-1}\mathbf{G}_i\mathbf{q} \qquad \text{for } i = 4, 5, 6 \text{ and } 7 \tag{25c}$$

$$\beta_i = \frac{1}{H_i}\mathbf{G}_i\mathbf{q} \qquad \text{for } i = 8, 9 \text{ and } 10. \tag{25e}$$

Further manipulations yield:

$$\lambda_i = \frac{\mathbf{R}_i^{\mathrm{T}}\mathbf{H}_i^{-1}\mathbf{G}_i}{\mathbf{R}_i^{\mathrm{T}}\mathbf{H}_i^{-1}\mathbf{R}_i}\mathbf{q};\quad \underline{\beta}_i = \left(\mathbf{H}_i^{-1} - \frac{(\mathbf{H}_i^{-1}\mathbf{R}_i)(\mathbf{H}_i^{-1}\mathbf{R}_i)^{\mathrm{T}}}{\mathbf{R}_i^{\mathrm{T}}\mathbf{H}_i^{-1}\mathbf{R}_i}\right)\mathbf{G}_i\mathbf{q} \quad \text{for } i = 1, 2 \text{ and } 3 \tag{26}$$

and

$$\Pi^e = \frac{1}{2}\mathbf{q}^{\mathrm{T}}\left\{\sum_{i=1}^{3}\mathbf{G}_i^{\mathrm{T}}\left(\mathbf{H}_i^{-1} - \frac{(\mathbf{H}_i^{-1}\mathbf{R}_i)(\mathbf{H}_i^{-1}\mathbf{R}_i)^{\mathrm{T}}}{\mathbf{R}_i^{\mathrm{T}}\mathbf{H}_i^{-1}\mathbf{R}_i}\right)\mathbf{G}_i + \sum_{i=4}^{7}\mathbf{G}_i^{\mathrm{T}}\mathbf{H}_i^{-1}\mathbf{G}_i\right.$$
$$\left. + \sum_{i=8}^{10}\frac{1}{H_i}\mathbf{G}_i^{\mathrm{T}}\mathbf{G}_i + \frac{1}{f_0}\mathbf{G}_c^{\mathrm{T}}\mathbf{S}^{-1}\mathbf{G}_c + \mathbf{K}_s\right\}\mathbf{q} - \mathbf{F}^{\mathrm{T}}\mathbf{q}. \tag{27}$$

The element stiffness matrix is apparently the one included by the braces. As $(\mathbf{R}_i^{\mathrm{T}}\mathbf{H}_i^{-1}\mathbf{R}_i)$'s are scalars, the only inversion cost is incurred by $\mathbf{H}_4$, $\mathbf{H}_5$, $\mathbf{H}_6$ and $\mathbf{H}_7$ which are 3×3 symmetric matrices.

8 Simplified evaluation of penalty stiffness

Since the roles of the penalty are to stabilize the element and to enforce the equality of the two rotations $\underline{\Omega}$ and $\underline{\omega}$, much freedom is available in its evaluation. To keep $\mathbf{K}_s$ efficient in formulation and effective in suppressing the six *equal-rotation* modes, only 6 integration points out of 14-point rule (Irons 1971) are employed for its evaluation. The natural coordinates of the employed integration points are:

$$(\pm b, 0, 0),\quad (0, \pm b, 0) \quad \text{and} \quad (0, 0, \pm b) \tag{28}$$

in which $b = 0.795822426$. The differences in rotations $\underline{\Omega}$ and $\underline{\omega}$ about the natural coordinate axes are first resolved, namely

$$\mathbf{g}_i(\underline{\omega}^u - \underline{\omega}) = \mathbf{g}_i(\mathbf{L}_r\mathbf{N}_t - \mathbf{N}_r)\mathbf{q} \tag{29}$$

where

$$\mathbf{g}_i = \frac{1}{(a_i^2 + b_i^2 + c_i^2)^{1/2}}[a_i \quad b_i \quad c_i]^T$$

and i equals 1, 2 and 3 for the difference in rotations about ξ-, η- and ζ-axis, respectively. The refined penalty stiffness would be:

$$\mathbf{K}_s = \mathbf{K}_{s1} + \mathbf{K}_{s2} + \mathbf{K}_{s3} \tag{30}$$

in which

$$\mathbf{K}_{si} = \gamma f_0 \sum (\mathbf{L}_r\mathbf{N}_t - \mathbf{N}_r)^T \mathbf{g}_i^T \mathbf{g}_i (\mathbf{L}_r\mathbf{N}_t - \mathbf{N}_r). \tag{31}$$

Summation is carried out over $(\pm b, 0, 0)$, $(0, \pm b, 0)$ and $(0, 0, \pm b)$ for $i = 1$, 2 and 3, respectively. Each of the $\mathbf{K}_{si}$'s serves to stabilize the two *equal-rotation* modes about the corresponding axis. In penalty formulations, the choice of the penalty factor are often controversial. However, we would simply follow the practice of Hughes and Brezzi (1989) and Ibrahimbegovic and Wilson (1991) in taking γ as the shear modulus, instead of optimizing γ with respect to any benchmark problems.

9 Numerical tests

Besides the present element, termed *HBR*, predictions of the following 8-node brick elements with rotational d.o.f. will also be included whenever possible:

(a) *AH* is the 42-β hybrid element developed by Yunus et al. (1989). No stabilization scheme against the *equal-rotation* modes was mentioned in reference. The 14-point integration rule is used.

(b) *HEX8RX* is the element devised by Yunus et al. (1991). Three internal displacement modes are assumed in the element and the two-point quadrature is employed for numerical integration. MacNeal and Harder's (1989) stabilization schemes are generalized to suppress the 6 *equal-rotation* modes and the 6 *hourglass* modes.

(c) *IBR-D* and *IBR-M* are Ibrahimbegovic and Wilson's elements (1991). Both elements employ the 14-point integration rule for their core stiffness matrices and the two-point quadrature for the penalty stiffness matrices.

Results of *AH*, *IBR-D* and *IBR-M* are all extracted from the corresponding references. Results of *HEX8RX* that cannot be found in (Yunus et al. 1991) are computed by using the commercial finite element package *ANSYS*. Designation of *HEX8RX* in *ANSYS Rev.4.4A* is *STIF73*.

Patch test, invariance and nodal numbering

HBR has been tested to be geometrically invariant, insensitive to different node numbering sequence and able to pass the generalized patch test. It is therefore consistent from the finite element point of view and of the correct rank, namely 42.

Simple beam problem

Figure 2 describes the problem. The applied moments are represented by (1) end bending forces $P/2$ and by (2) nodal couples $M/2$ at all end nodes. Load case (3) simulates the situation when a plate/shell element is connected to the end sections. For case (1), zero rotations ω_y and ω_z are restrained so that the nodal couples obtained by discretizing the distributed bending stress need

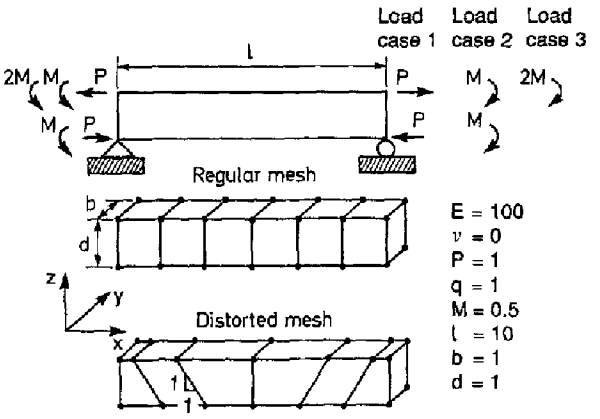

Fig. 2. A simple beam

not be prescribed. For convenience, the same displacement boundary conditions would be applied for cases (2) and (3). Normalized midspan deflections and end rotations are listed in Table 1 for cases (1) and (2). It can be seen that *HBR* is least susceptible to mesh distortion and is accurate in both deflection and rotation, particularly under the couple load. *HEX8RX* is poor in rotation under the couple load. For load case (3), only the regular mesh is employed but the beam depth d is varied. In view of the normalized predictions in Table 2, it is advisable to interface plate/shell elements with thin solid elements with rotational d.o.f.

Simply supported square plate problem

This problem is illustrated in Fig. 3. The plate is subjected to a uniform transverse loading of intensity $q = 1$. Owing to symmetry, only a quarter of the plate is analyzed by either a 2×2 mesh or a 4×4 mesh. Central deflections are normalized by the series solutions cited in (Ibrahimbegovic

Table 1. Normalized mid-span deflection and end rotation for simple beam problem, load cases (1) and (2), Fig. 2

Element	Regular mesh Load case (1)		Load case (2)		Distorted mesh Load case (1)		Load case (2)	
	Deflect.	Rotat.	Deflect.	Rotat.	Deflect.	Rotat.	Deflect.	Rotat.
IBR-D	1.000	1.000	1.000	1.074	0.848	0.880	0.853	1.041
IBR-M	1.000	1.000	1.000	1.050	0.882	0.946	0.885	1.092
HEX8RX	1.000	1.000	1.000	1.720	0.966	0.827	0.814	1.512
HBR	1.000	1.000	1.007	1.060	0.945	0.937	0.942	1.020
Theory	1.5	0.6	1.5	0.6	1.5	0.6	1.5	0.6

Table 2. Normalized mid-span deflection and end rotation with varying depth d for simple beam problem, load case (3), regular mesh, Fig. 2

Depth d	*HED8RX*		*HBR*	
	Deflect.	Rotat.	Deflect.	Rotat.
1.0	1.025	1.991	1.027	1.283
0.5	1.002	1.220	1.004	1.054
0.1	1.000	1.008	1.000	1.001
Theory [d^3]	1.5	0.6	1.5	0.6

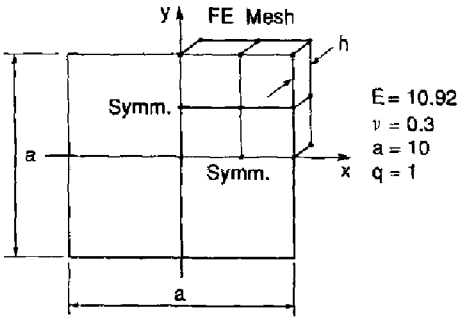

Fig. 3. Simply supported square plate with uniform loading

Table 3. Normalized central deflection for simply supported square plate, Fig. 3

Element	$h = 1$		$h = 0.1$	
	2 × 2 mesh	4 × 4 mesh	2 × 2 mesh	4 × 4 mesh
IBR-D	0.942	0.986	0.569	0.782
IBR-M	0.959	0.986	0.583	0.806
HEX8RX	1.033	—	0.981	—
HBR	0.995	1.027	0.717	0.991
Series solution	42.728	42.728	40644	40644

and Wilson 1991). The results are given in Table 3. *HEX8RX* is less susceptible to shear locking than *HBR*. This is due to the strong penalty (roughly, 10^6 times of the penalty employed in *HEX8RX*) employed in penalty matrix.

Slender beam problem

Figure 4 shows a slender straight beam subjected to unit inplane and unit out-of-plane end shear forces. In all distorted meshes, the nodes are shifted from their regular positions by 0.1 unit along the centroidal axis. All d.o.f. at the clamped end are restrained to zero. Normalized beam tip deflections in direction of the applied loads and the reference solutions given by MacNeal and Harder (1985) are listed in Table 4. The present *HBR* is least susceptible to mesh distortions.

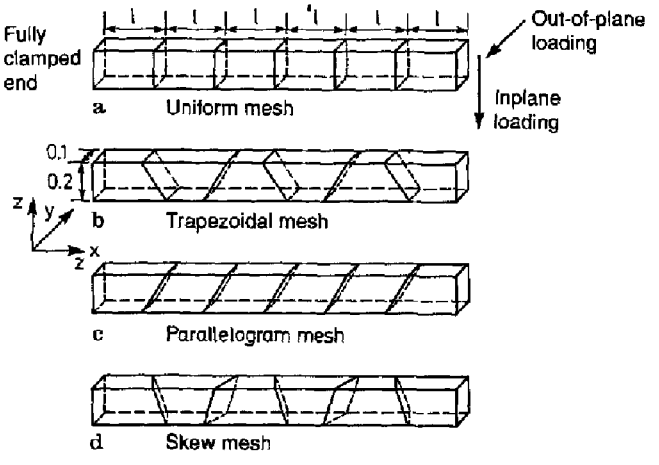

Fig. 4a–d. MacNeal's slender beam problem, $E = 10^7$, $\nu = 0.3$

Table 4. Normalized predictions for straight beam problems, Fig. 4

Element	Inplane loading				Out-of-plane loading			
	Reg.	Trape.	Para.	Skew	Reg.	Trape.	Para.	Skew
AH	0.898	0.860	0.870	—	0.888	0.868	0.878	—
HEX8RX	0.988	0.863	0.921	0.949	0.983	0.943	0.969	0.856
HBR	0.989	0.938	0.935	0.960	0.984	0.923	0.969	0.930
Reference	1.081				0.4321			

Curved and twisted beam problems

Curved beam and the twisted beam problems are depicted in Figs. 5 and 6, respectively. Same as the slender beam problem, all nodal d.o.f. at the clamped ends are deleted. The normalized predictions are given in Table 5. The reference solutions are quoted from (MacNeal and Harder 1985). Accuracy of *HEX8RX* and *HBR* are extremely close except for the curved beam problem with out-of-plane loading. This is again caused by the strong penalty in *HBR*. It has been checked that if the penalty in *HBR* is reduced by 10^6 times (same order of magnitude as that in *HEX8RX*), an accuracy of 0.90 can be obtained.

Plane wedge problem

The popular plane wedge problem is shown in Fig. 7. Shear force of unit magnitude is uniformly distributed over the free end of the wedge. All d.o.f. at the clamped end are deleted. The normalized

Table 5. Normalized predictions for curved and twisted beams, Figs. 5 and 6

Element	Inplane loading		Out-of-plane loading	
	Curved beam	Twisted beam	Curved beam	Twisted beam
AH	0.969	—	0.896	—
HEX8RX	0.997	1.001	0.890	0.999
HBR	0.998	1.002	0.818	1.001
Reference	0.08734	0.005424	0.5022	0.001754

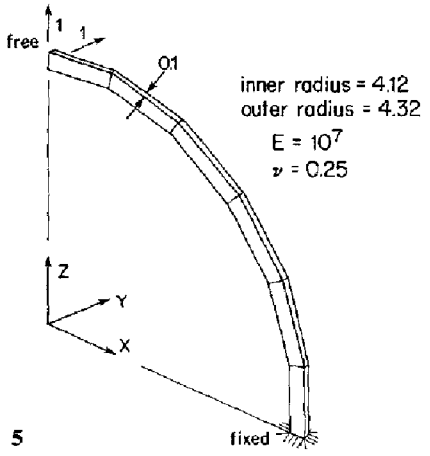

5

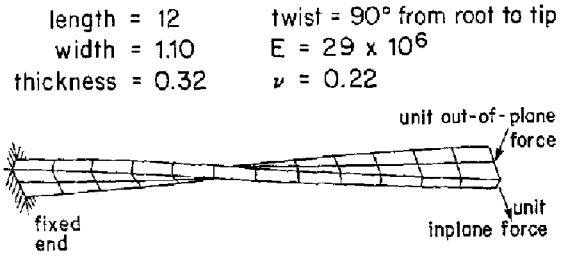

6

Figs. 5 and 6. 5 Curved beam problem, 6 twisted beam problem

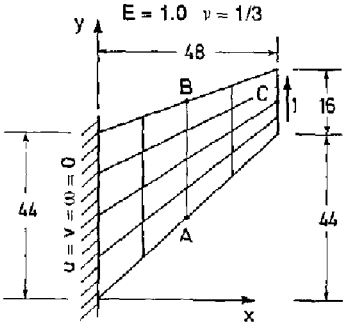

Fig. 7. Plane wedge problem (4 × 4 mesh)

Table 6. Normalized predictions for plane wedge problem, Fig. 7

Element	2 × 2 mesh			4 × 4 mesh		
	v_c	$\sigma_{A(\max)}$	$\sigma_{B(\min)}$	v_c	$\sigma_{A(\max)}$	$\sigma_{B(\min)}$
HED8RX	0.911	0.779	0.977	0.964	0.963	0.964
HBR	0.914	0.796	0.936	0.968	0.960	0.952
Best known	23.90	0.2360	−0.2010	23.90	0.2360	−0.2010

predictions for the upward deflection at C, maximum principal stress at A and minimum principal stress at B are listed in Table 6. The best known solution is quoted from (Cook 1986). Once again, *HEX8RX* and *HBR* yield close accuracy.

Two-element cantilever beam—effect of element distortion

Except for the predictions in rotations under point couple loading, the present *HBR* and *HEX8RX* yield close accuracy. It is mainly because the considered meshes are largely restricted to prismatic shape which is highly symmetric for solid elements. Effect of the *chisel-shaped* distortion is

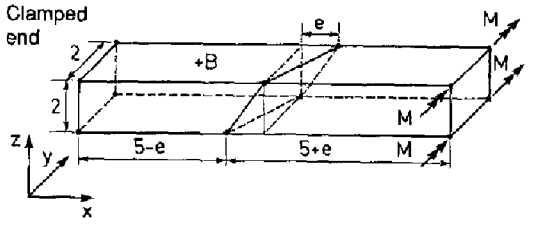

Fig. 8. Two-element cantilever beam, $M = 1000$, $E = 1500$, $\nu = 0.25$

Table 7. Normalized predictions for two-beam cantilever beam, Fig. 8

e	*HEX8RX*			*HBR*			*HBR* without *AMF*		
	Deflect.	Rotat.	σ_{xx}	Deflect.	Rotat.	σ_{xx}	Deflect.	Rotat.	σ_{xx}
0	0.988	1.393	1.000	0.996	1.044	1.004	0.996	1.044	1.004
1	0.920	1.354	0.881	0.971	1.041	1.027	0.975	1.041	0.975
2	0.760	1.258	0.683	0.890	1.033	0.961	0.904	1.030	0.884
3	0.573	1.149	0.498	0.750	1.019	0.800	0.766	0.990	0.728
Reference	−100	20	3000	−100	20	300	−100	20	3000

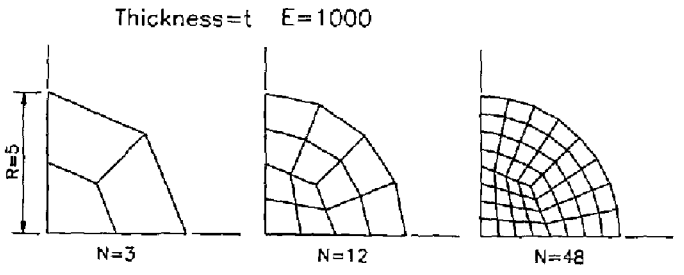

Fig. 9. Meshes for modeling quadrant of a circular plate, $\nu = 0.3, 0.49, 0.4999$

Table 8. Normalized central deflections for clamped circular plate, Fig. 9

Element	$\nu = 0.3; h = 0.1$			$h = 0.1; N = 12$	
	$N = 3$	$N = 12$	$N = 48$	$\nu = 0.49$	$\nu = 0.4999$
HEX8RX	—	0.850	—	0.670	0.036
HBR	0.208	0.832	0.967	0.848	0.849
Reference $[h^3]$		5431		4535	4477

considered by using the two-element cantilever beam problem shown in Fig. 8. At the clamped end, all nodal d.o.f. are restrained. Bending stress σ_{xx} at the element face centre B, end deflection and end rotation are computed. Their normalized values are given in Table 7. It can be seen that *HBR* is much less susceptible to distortion than *HEX8RX*. Results of the unsimplified *HBR* in which *admissible matrix formulation* (*AMF*) is not applied are also included to examine its effect. While the unsimplified *HBR* is slightly more accurate in deflection and rotation, it is less accurate in the bending stress.

Clamped circular plate and volumetric locking

Three different meshes are employed to model a quadrant of a clamped circular plate, see Fig. 9. The plate is subjected to a unit transverse central point load. In the clamped periphery, all nodal d.o.f. are restrained. Results for the convergence study for thickness $h = 0.1$ and Poisson's ratio $\nu = 0.3$ is listed in Table 8. Finally, the Poisson's ratio is set to 0.49 and 0.4999. Only the mesh with medium density is considered. *HEX8RX* exhibits the volumetric locking as noted in the table. The reference solution is quoted by Timoshenko and Woinowsky-Krieger (1970).

11 Conclusions

A 8-node hybrid brick element with rotational d.o.f. is presented. The element is rank sufficient, geometrically invariant and insensitive to different node numbering schemes. The element is also free from volumetric and trapezoidal lockings. The six *equal-rotation* spurious zero energy modes intrinsic to Allman's interpolation are suppressed by using a penalty stiffness. The latter enforces the equality of the nodal rotation and the continuum-defined rotation. For the chosen penalty parameter, close agreement of the nodal rotation and the continuum-defined rotation is achieved. Compared to other elements in the open literature, this element is least susceptible to mesh distortion.

An efficient computational scheme, based on the *admissible matrix formulation* (Sze 1992) and stress constraints, is suggested. To invert the flexibility matrix for the effectively 36-β stress field, only four 3×3 symmetric matrices have to be inverted.

Acknowledgement

This research was partially completed when the first author, K. Y. Sze, was a Croucher Foundation postdoctoral fellow at the University of Calgary.

Appendix: Shape function matrix $\mathbf{N}_t$

Before giving out the displacement shape function matrix $\mathbf{N}_t$ explicitly, the following quantities are defined:

$$N_i = \frac{1}{8}(1+\xi_i\xi)(1+\eta_i\eta)(1+\zeta_i\zeta), \quad x_{ij} = x_i - x_j, \quad y_{ij} = y_i - y_j, \quad z_{ij} = z_i - z_j$$

$$M_1 = \frac{1}{8}(1-\xi^2)(1+\eta)(1+\zeta) \quad M_2 = \frac{1}{8}(1-\xi)(1-\eta^2)(1+\zeta) \quad M_3 = \frac{1}{8}(1-\xi^2)(1-\eta)(1+\zeta)$$

$$M_4 = \frac{1}{8}(1+\xi)(1-\eta^2)(1+\zeta) \quad M_5 = \frac{1}{8}(1+\xi)(1+\eta)(1-\zeta^2) \quad M_6 = \frac{1}{8}(1-\xi)(1+\eta)(1-\zeta^2)$$

$$M_7 = \frac{1}{8}(1-\xi)(1-\eta)(1-\zeta^2) \quad M_8 = \frac{1}{8}(1+\xi)(1-\eta)(1-\zeta^2) \quad M_9 = \frac{1}{8}(1-\xi^2)(1+\eta)(1-\zeta)$$

$$M_{10} = \frac{1}{8}(1-\xi)(1-\eta^2)(1-\zeta) \quad M_{11} = \frac{1}{8}(1-\xi^2)(1-\eta)(1-\zeta) \quad M_{12} = \frac{1}{8}(1+\xi)(1-\eta^2)(1-\zeta).$$

In N_i, (ξ_i, η_i, ζ_i) is the natural coordinates of the i-th node, $\mathbf{N}_t$ can then be partitioned as:

$$\mathbf{N}_t = [N_1\mathbf{I}_3 \quad \mathbf{M}_1 \quad N_2\mathbf{I}_3 \quad \mathbf{M}_2 \quad \cdots \quad N_7\mathbf{I}_3 \quad \mathbf{M}_7 \quad N_8\mathbf{I}_3 \quad \mathbf{M}_8]$$

in which

$$\mathbf{M}_1 = \begin{bmatrix} 0 & z_{21}M_1 - z_{14}M_4 + z_{51}M_5 & -y_{21}M_1 + y_{14}M_4 - y_{51}M_5 \\ -z_{21}M_1 + z_{14}M_4 - z_{51}M_5 & 0 & x_{21}M_1 - x_{14}M_4 + x_{51}M_5 \\ y_{21}M_1 - y_{14}M_4 + y_{51}M_5 & -x_{21}M_1 + x_{14}M_4 - x_{51}M_5 & 0 \end{bmatrix}$$

$$\mathbf{M}_2 = \begin{bmatrix} 0 & z_{32}M_2 - z_{21}M_1 + z_{62}M_6 & -y_{32}M_2 + y_{21}M_1 - y_{62}M_6 \\ -z_{32}M_2 + z_{21}M_1 - z_{62}M_6 & 0 & x_{32}M_2 - x_{21}M_1 + x_{62}M_6 \\ y_{32}M_2 - y_{21}M_1 + y_{62}M_6 & -x_{32}M_2 + x_{21}M_1 - x_{62}M_6 & 0 \end{bmatrix}$$

$$\mathbf{M}_3 = \begin{bmatrix} 0 & z_{43}M_3 - z_{32}M_2 + z_{73}M_7 & -y_{43}M_3 + y_{32}M_2 - y_{73}M_7 \\ -z_{43}M_3 + z_{32}M_2 - z_{73}M_7 & 0 & x_{43}M_3 - x_{32}M_2 + x_{73}M_7 \\ y_{43}M_3 - y_{32}M_2 + y_{73}M_7 & -x_{43}M_3 + x_{32}M_2 - x_{73}M_7 & 0 \end{bmatrix}$$

$$\mathbf{M}_4 = \begin{bmatrix} 0 & z_{14}M_4 - z_{43}M_3 + z_{84}M_8 & -y_{14}M_4 + y_{43}M_3 - y_{84}M_8 \\ -z_{14}M_4 + z_{43}M_3 - z_{84}M_8 & 0 & x_{14}M_4 - x_{43}M_3 + x_{84}M_8 \\ y_{14}M_4 - y_{43}M_3 + y_{84}M_8 & -x_{14}M_4 + x_{43}M_3 - x_{84}M_8 & 0 \end{bmatrix}$$

$$\mathbf{M}_5 = \begin{bmatrix} 0 & -z_{51}M_5 + z_{65}M_9 - z_{58}M_{12} & y_{51}M_5 - y_{65}M_9 + y_{58}M_{12} \\ z_{51}M_5 - z_{65}M_9 + z_{58}M_{12} & 0 & -x_{51}M_5 + x_{65}M_9 - x_{58}M_{12} \\ -y_{51}M_5 + y_{65}M_9 - y_{58}M_{12} & x_{51}M_5 - x_{65}M_9 + x_{58}M_{12} & 0 \end{bmatrix}$$

$$\mathbf{M}_6 = \begin{bmatrix} 0 & -z_{62}M_6 + z_{76}M_{10} - z_{65}M_9 & y_{62}M_6 - y_{76}M_{10} + y_{65}M_9 \\ z_{62}M_6 - z_{76}M_{10} + z_{65}M_9 & 0 & -x_{62}M_6 + x_{76}M_{10} - x_{65}M_9 \\ -y_{62}M_6 + y_{76}M_{10} - y_{65}M_9 & x_{62}M_6 - x_{76}M_{10} + x_{65}M_9 & 0 \end{bmatrix}$$

$$\mathbf{M}_7 = \begin{bmatrix} 0 & -z_{73}M_7 + z_{87}M_{11} - z_{76}M_{10} & y_{73}M_7 - y_{87}M_{11} + y_{76}M_{10} \\ z_{73}M_7 - z_{87}M_{11} + z_{76}M_{10} & 0 & -x_{73}M_7 + x_{87}M_{11} - x_{76}M_{10} \\ -y_{73}M_7 + y_{87}M_{11} - y_{76}M_{10} & x_{73}M_7 - x_{87}M_{11} + x_{76}M_{10} & 0 \end{bmatrix}$$

$$\mathbf{M}_8 = \begin{bmatrix} 0 & -z_{84}M_8 + z_{58}M_{12} - z_{87}M_{11} & y_{84}M_8 - y_{58}M_{12} + y_{87}M_{11} \\ z_{84}M_8 - z_{58}M_{12} + z_{87}M_{11} & 0 & -x_{84}M_8 + x_{58}M_{12} - x_{87}M_{11} \\ -y_{84}M_8 + y_{58}M_{12} - y_{87}M_{11} & x_{84}M_8 - x_{58}M_{12} + x_{87}M_{11} & 0 \end{bmatrix}$$

References

Atluri, S. N. (1979): On rate principles for finite strain analysis of elastic and nonelastic solids. Recent Research of Mechanical Behaviour of Solids, 79–107 (Professor H. Miyamoto's Anniversary Volume), University of Tokyo Press

Atluri, S. N. (1980): On some new general and complementary energy principles for the rate problems of finite strain, classic plasticity. J. Struct. Mech. 8, 61–92

Allman, D. J. (1984): A compatible triangular element including vertex rotations for plane elasticity analysis, Comp. and Struct. 19, 1–8

Bergan, P. G.; Felippa, C. A. (1985): A triangular membrane element with rotational degrees of freedom. Comp. Meth. Appl. Mech. Engng. 50, 25–69

Cook, R. D. (1986): On the Allman triangle and a related quadrilateral element. Comp. and Struct. 22, 1065–1067

Cook, R. D.; Malkus, D. S.; Plesha, M. E. (1989): Concepts and applications of finite element analysis, 3rd edn. John Wiley & Sons

Hughes, T. J. R.; Brezzi, F. (1989): On drilling degrees of freedom. Comp. Meth. Appl. Mech. Engng. 72, 105–121

Ibrahimbegovic, A.; Wilson, E. L. (1991): Thick shell and solid finite elements with independent rotation fields. Int. J. Num. Meth. Engng. 31, 1393–1414

Irons, B. M. (1971): Quadrature rules for brick based finite elements. Int. J. Num. Meth. Engng. 3, 293–294 (1971)

Irons, B. M.; Ahmad, S. (1980): Techniques of finite elements, Ellis Horwood

Iura, M.; Atluri, S. N. (1992): Formulation of a membrane finite element with drilling degrees of freedom. Comput. Mech. 9, 412–428

MacNeal, R. H.; Harder, R. L. (1985): A proposed standard set of problems to test finite element accuracy. Finite Elements in Analysis and Design 1, 3–20

MacNeal, R. H.; Harder, R. L. (1989): A refined four-noded membrane element with rotational degrees of freedom. Comp. and Struct. 28, 75–84

Pawlak, T. P.; Yunus, S. M.; Cook, R. D. (1991): Solid elements with rotational degrees of freedom: part II—tetrahedron elements. Int. J. Num. Meth. Engng. 31, 539–610

Pian, T. H. H.; Tong, P. (1969): Basis of finite element methods for solid continua. Int. J. Num. Meth. Engng. 1, 3–28

Pian, T. H. H.; Chen, D.-P.; Kang, D. (1983): A new formulation of hybrid/mixed finite element methods. Comp. and Struct. 16, 81–87

Pian, T. H. H.; Chen, D.-P. (1983): On the suppression of zero energy deformation modes. Int. J. Num. Meth. Engng. 19, 1741–1752

Pian, T. H. H.; Sumihara, K. (1984): Rational approach for assumed stress finite elements. Int. J. Num. Meth. Engng. 20, 1685–1695

Punch, E. F.; Atluri, S. N. (1984): Applications of isoparametric three-dimensional hybrid-stress finite elements with least-order stress fields. Comp. and Struct. 19, 409–430

Reissner, E. (1986): Some aspects of the variational principles problem in elasticity. Comput. Mech. 1, 3–9

Rubinstein, R.; Punch, E. F.; Atluri, S. N. (1983): An analysis of, and remedies for, kinematic modes in hybrid-stress finite elements: selection of stable, invariant stress fields. Comp. Meth. Appl. Mech. Engng. 38, 63–92

Sze, K. Y.; Chow, C. L. (1991a): An incompatible element for axisymmetric structure and its modification by hybrid method. Int. J. Num. Meth. Engng. 31, 385–405

Sze, K. Y.; Chow, C. L. (1991b): An efficient hybrid quadrilateral Kirchhoff plate bending element. Int. J. Num. Meth. Engng. 32, 149–169

Sze, K. Y. (1992): Efficient formulation of robust hybrid elements using orthogonal stress/strain interpolants and admissible matrix formulation. Int. J. Num. Meth. Engng. 35, 1–20

Sze, K. Y.; Chow, C. L.; Chen, W.-J. (1992): On invariance of isoparametric hybrid elements. Commun. Appl. Num. Meth. 8, 385–406

Sze, K. Y.; Chen, W.-J.; Cheung, Y. K. (1992): An efficient quadrilateral plane element with drilling degrees of freedom using orthogonal stress modes. Comp. and Struct. 42, 695–705

Sze, K. Y.; Ghali, A. (1992): Hybrid plane quadrilateral element with corner rotations. ASCE—J. Struct. Engng., accepted for publication

Taylor, R. L.; Simo, J. C.; Zienkiewicz, O. C.; Chan, C. H. (1986): The patch test—a condition for assessing fem convergence. Int. J. Num. Meth. Engng. 22, 39–62

Timoshenko, S. P.; Woinowsky-Krieger, S. (1970): Theory of plates and shells, 2nd edn. McGraw-Hill

Yunus, S. M.; Saigal, S., Cook, R. D. (1989): On improved hybrid finite elements with rotational degrees of freedom. Int. J. Num. Meth. Engng. 28, 785–800

Yunus, S. M.; Pawlak, T. P.; Cook; R. D. (1991): Solid elements with rotational degrees of freedom: part 1—hexahedron elements. Int. J. Num. Meth. Engng. 31, 573–592

Communicated by S. N. Atluri, September 12, 1992